Journal of Power Sources 195 (2010) 4168–4176

Contents lists available at ScienceDirect

Journal of Power Sources

journal homepage: www.elsevier.com/locate/jpowsour

Two-phase flow pressure drop hysteresis in parallel channels of a proton exchange membrane fuel cell

Ryan Anderson, David P. Wilkinson*, Xiaotao Bi, Lifeng Zhang

Department of Chemical and Biological Engineering, University of British Columbia, Clean Energy Research Centre, 2360 East Mall Vancouver, BC, Canada, V6T 1Z3

ARTICLE INFO

Article history:
Received 6 December 2009
Received in revised form
23 December 2009
Accepted 29 December 2009
Available online 13 January 2010

Keywords:
Two-phase flow
Hysteresis
PEM fuel cell
Water management

ABSTRACT

Two-phase flow pressure drop hysteresis was studied in a non-operational PEM fuel cell to understand the effect of stoichiometry, GDL characteristics, operating range, and initial conditions (dry vs. flooded) for flow conditions typical of an operating fuel cell. This hysteresis is noted when the air and water flow rates are increased and then decreased along the same path, exhibiting different pressure drops. When starting from dry conditions, the descending pressure drop tended to be higher than the ascending pressure drop at lower simulated current densities. The hysteresis effect was noted for stoichiometries of 1–4 and was eliminated at a stoichiometry of 5. It was found that the hysteresis was greater when water breakthrough occurred at higher simulated current densities, which is a function of GDL properties. The operating range had to reach a critical simulated current density (800 mA cm^{-2} in this case) between the ascending and descending approach to create a pressure drop hysteresis zone. The descending step size does not change the size of the hysteresis effect, but a larger step size leads to lower fluctuations in the pressure drop signal. An initially flooded condition also showed hysteresis, but the ascending approach tended to have a higher pressure drop than the descending approach.

1. Introduction

The proton exchange membrane (PEM) fuel cell has received much attention in recent decades as a clean and efficient way to generate power. Advantages include high energy efficiency, low operating temperature, and little to zero emissions during its operation. Although a promising energy conversion device, several technical concerns still impede further use of fuel cells in practical applications. One major issue that has received a great deal of attention is the proper water management of the fuel cell.

A recent review [1] has detailed issues associated with water management and describes how the catalyst layer, gas diffusion layer (GDL), and flow field channels of the PEM fuel cell are prone to flooding. The paper also detailed mitigation strategies based on engineering design, optimizing operating conditions, and material modifications. While comprehensive in the overall picture of water management, little emphasis has been placed on gas–liquid two-phase flow issues in the flow field channel itself. Two-phase flow in PEM fuel cells is a complicated phenomenon, but a full understanding of it is important for the comprehensive understanding of fuel cell water management [2,3]. This complexity includes large gas to liquid ratios, water produced by electrochemical reaction entering the flow field channels from a porous wall (GDL), and water entering the flow field channels from the condensation of humidified gas reactants. Water introduction from the porous GDL is different from traditional two-phase flow studies [4–7], where the two phases are typically introduced together or mixed before the inlet. This difference makes two-phase flow studies in fuel cell flow channels particularly unique.

Liquid water is a major problem in fuel cells because several problems can emerge [3] including: blockage of the channel by liquid water, which can increase the pressure drop in the channel, non-uniform current distribution, and a liquid film developing on the GDL surface, which blocks reactant gas from reaching reaction sites.

To address two-phase flow in flow field channels in a simplified setup, non-operating experiments [8–10] can be run to mimic the behavior of operating fuel cells [11–13]. Non-operating experiments possess the advantage of being able to control relevant operating conditions while decoupling reaction and heat/mass transfer from the hydrodynamics. In general, water in non-operating experiments is injected through a GDL into the air flow field channel (simulating the cathode flow field channel) to observe relevant two-phase flow behavior. Borrelli et al. [8] showed that the non-operating experiments exhibit similar droplet behavior to operating cells, with droplets growing at preferred locations before detachment, and that the GDL type influences the water removal

* Corresponding author. Tel.: +1 604 822 4888; fax: +1 604 822 6003.
E-mail addresses: dwilkinson@chbe.ubc.ca, dwilkinson@chml.ubc.ca (D.P. Wilkinson).

0378-7753/$ – see front matter © 2010 Elsevier B.V. All rights reserved.
doi:10.1016/j.jpowsour.2009.12.134

Nomenclature

c_P	specific heat ($J\,g^{-1}\,K^{-1}$)
F	Faraday's constant (96,485.339 $C\,mol^{-1}$)
I	current (A)
i	current density ($A\,cm^{-2}$)
k	ratio of specific heats (diatomic gas = 1.4)
$\dot{m}$	mass flow rate ($g\,s^{-1}$)
$\dot{N}$	molar flow rate ($mol\,s^{-1}$)
ΔP	pressure drop (Pa)
T	temperature (K)
W	power ($W\,cm^{-2}$)

Greek letters

ρ	density ($g\,cm^{-3}$)
λ_i	stoichiometric ratio of gas i

Subscripts

comp	compressor
$O_{2,need}$	required oxygen demand at a given current density
$O_{2,inlet}$	supplied oxygen demand at a given current density

process. However, the preferential breakthrough location may be dynamic and an interconnected network of pathways in the GDL may exist [9], complicating the emergence of two-phase flow.

Once the droplets emerge into the flow field channels, non-operating experiments have shown various two-phase flow patterns including slug, film, corner, and mist flows depending on the superficial air velocity and GDL properties [10]. Film flow or stratified flow is considered to be a desirable pattern in fuel cells because water is only covering the channel walls, leaving the GDL surface exposed for gas diffusion. However, the superficial velocity needed to achieve this flow pattern varies with experimental setup, with Trabold et al. [2] pointing out that a superficial gas velocity of 5–6 $m\,s^{-1}$ is needed and Lu et al. [14] recommending more than 3 $m\,s^{-1}$. The value of the needed superficial velocity may also change with operating current density [15].

Recently, two-phase flow pressure drop hysteresis phenomena were found when the flow rate of air was changed in an ascending or a descending manner for a set liquid water injection rate [16,17]. The results were obtained from an experimental setup with water and air introduced together at the inlet of parallel minichannels. Flow hysteresis is also observed in minichannels bounded with porous walls [18], where the transitions between flow regimes showed substantial hysteresis depending on whether the air flow rate was varied in an ascending or descending manner. This is an important consideration in fuel cell applications such as transportation, where the duty cycle can cover a wide range of operating conditions and require ascending and descending power operation [19].

Two-phase flow hysteresis can lead to an unexpectedly high pressure drop, decreasing fuel cell efficiency due to the associated parasitic power loss. A different pressure drop path as the current density is cycled (air and water flows changing in an ascending and descending manner) can also alter the specific two-phase flow pattern, which may have implications in how water is removed and how effectively the oxygen in air can reach the cathode catalyst layer.

This paper explores pressure drop hysteresis in a non-operating fuel cell. Evidence of pressure drop hysteresis is noted in the operating fuel cell case, which necessitated a more detailed hydrodynamic study in the non-operating apparatus. The non-operating approach taken here injects water through a GDL into a cathode flow field channel with gases that are neither humidified nor heated. To understand the principles of this hysteresis behavior, the non-operating approach examined several variables including: the effect of air stoichiometry (Section 3.2), the GDL treatment (PTFE content and the inclusion of a MPL; Section 3.3), the range of current densities (Section 3.4), the effect of decreasing step size (Section 3.5), and the effect of initial state (dry vs. flooded; Section 3.6).

2. Experimental methods

The non-operating (no electrochemical reaction) experiments used the same fuel cell hardware and components as the fuel cell to be used in further operating (electrochemical) experiments. The anode and cathode flow field channels contain four parallel square channels that are each 1 mm × 1 mm in cross-section and 30 cm long with 1 mm landing widths. The fuel cell active area is 35.7 cm^2. An optically clear manifold allows for direct visual observation of the cathode flow field channels. The fuel cell used in this study is shown schematically in Fig. 1a and the non-operating experimental setup is shown in Fig. 1b.

The non-operating cell was run at ambient temperature, the cathode exit was at atmospheric pressure, and the cell was compressed to 105 psi_g. Air (Praxair Al 0.0XD Extra Dry) was not humidified or heated, with its flow rate controlled by a rotameter. The air entered the cathode manifold where it was distributed to the flow field channels before leaving from the cathode manifold exit. A GDL was placed between the anode and cathode flow field plates to mimic the actual water injection methods and surface

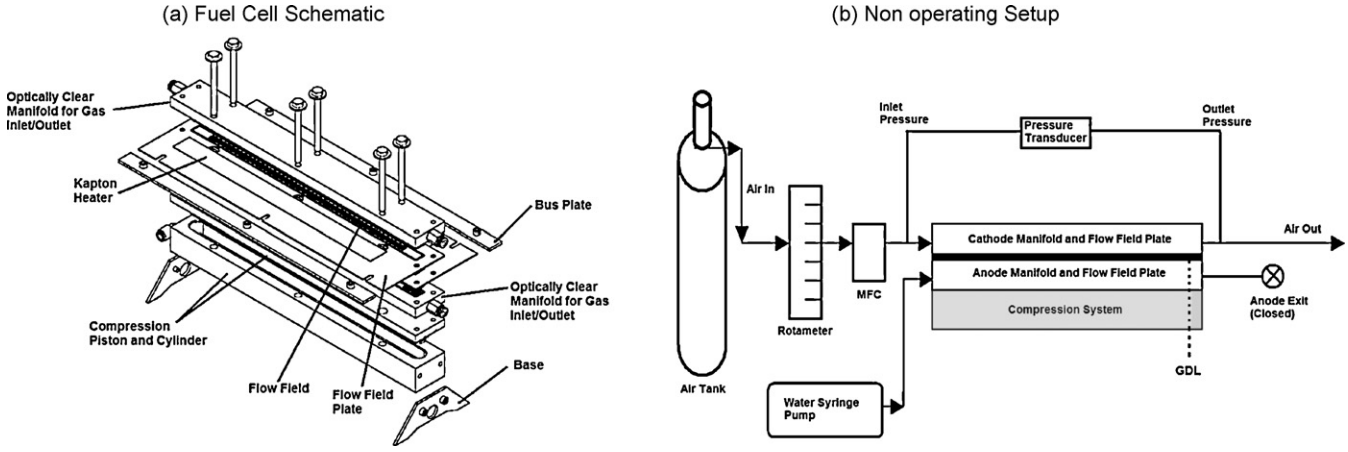

Fig. 1. (a) Fuel cell schematic and (b) non-operating setup.

Table 1
Gas diffusion layers and specifications.

Company	GDL	MPL	PTFE content	Thickness (μm)
SGL Carbon	25 BC	Yes	5%	235
SGL Carbon	25 BA	No	5%	190
SGL Carbon	25 DC	Yes	20%	231
Toray	TGPH-030	No	20%	110
Toray	TGPH-030	No	0%	110

properties of an operational fuel cell. The water was pumped into the anode flow field via a syringe pump (Cole-Parmer 780100C), and then was forced through the GDL as the syringe pumped at a given volumetric flow rate ($mL\,h^{-1}$). The anode exit was closed, allowing the water pumped into the anode to reach the cathode.

The GDLs and relevant specifications are shown in Table 1.

The water injection rate and needed air flow rate are governed at each current density by Faraday's law. For instance, the rate of water generation in $mol\,s^{-1}\,cm^{-2}$ is given by

$$N_{H_2O,generated} = \frac{I}{2F} \quad (1)$$

where I is the current (A) and F is the Faraday's constant. In this way, the corresponding water injection rate and necessary cathode air flow rate were set for a given current density. A stoichiometry, λ, of 1 refers to the minimum air flow needed for the electrochemical reaction defined by Faraday's law. The stoichiometric ratio is defined in Eq. (2):

$$\lambda = \frac{m_{O_2,inlet}}{m_{O_2,need}} \quad (2)$$

All stoichiometries here refer only to air on the cathode side (no hydrogen was used in the non-operating tests). For example, a stoichiometry of 2 uses the same liquid water injection rate at a given current density as a stoichiometry of 1, but with twice the air flow rate.

The air flow rate and water injection rates for the simulated current densities were run in both an ascending and descending manner to determine the extent of hysteresis in the two-phase pressure drop. Unless otherwise noted, each channel was purged with air before a trial to ensure a dry (single-phase) initial condition. In each experiment, the gas and water flow rates were first increased in an ascending manner at simulated current densities 50, 100, 200, 400, 600, and 800 $mA\,cm^{-2}$ and then decreased along the same path, corresponding to simulated current densities 600, 400, 200, 100, and 50 $mA\,cm^{-2}$. The incremental paths used for the ascending and descending current densities are referred to as the ascending approach and the descending approach. The pressure drop curve resulting from the ascending approach is referred to as the 'ascending pressure drop', and the pressure drop curve resulting from the descending approach is referred to as the 'descending pressure drop'. The magnitude of the incremental change in simulated current density is the 'step size' (a change from 400 $mA\,cm^{-2}$ to 600 $mA\,cm^{-2}$ is an ascending step size of 200 $mA\,cm^{-2}$). The flow rates at each simulated current density were held for approximately 8 min (approximate due to manually changing the flow rate of air and water), which gives the pressure drop sufficient time to reach a steady state, and the pressure transducer signal was sampled at 20 Hz.

3. Results and discussion

3.1. Pressure drop hysteresis in an operating fuel cell

The presence of two-phase flow hysteresis was first noted in the operating fuel cell under baseline operating conditions. The hysteresis in the operating cell motivated the further study in the non-operating mode. The conditions of the operating baseline are listed in Table 2.

Table 2
Operating fuel cell baseline conditions.

Operating variable	Baseline value
P_{gas}	206.8 kPa
T_{cell}, T_{gas}, T_{dp}	75 °C
Relative humidity	100%
$\lambda_{air}/\lambda_{H_2}$	2.0/1.5
Anode GDL	25 BA
Cathode GDL	25 BC
CCM	5010 Gore (0.4 $mg\,cm^{-2}$ Pt – both sides)
Oxidant gas	Air
Flow fields	4 parallel, square channels: co-flow

The polarization curve and ascending/descending pressure drop results for the operating fuel cell are shown in Fig. 2. All operating conditions were controlled with a Hydrogenics 2 kW fuel cell test station (Model No. G100). These polarization curves and pressure drop curves were obtained following both an ascending and descending path of current densities. The error bars represent the standard deviation of each data set.

A clear difference between the ascending and descending pressure drop is seen below current densities of 200 $mA\,cm^{-2}$, which is referred to as two-phase flow pressure drop hysteresis. To determine a hydrodynamic baseline for comparison to electrochemically driven two-phase flow studies in the future, further investigations were conducted with the same unit in a non-operating mode.

3.2. Effect of stoichiometry in the non-operating fuel cell

The gas stoichiometry can be used to convectively remove water in PEM fuel cell flow channels, and fuel cell channel flooding is particularly noted at low flow rates corresponding to low current densities [20]. The ascending and descending pressure drop results for stoichiometries of 1–5, which cover a typical range of fuel cell operations [11], are shown in Fig. 3. SGL 25 BC was chosen as the GDL because it is the one used on the cathode side of the operating fuel cell. The experimental conditions are those discussed in Section 2. Triplicate experiments were done at each current density, and these are the values reported in Fig. 3a. The error bars included for a stoichiometry of 1 are from the standard deviation of the three trials. Fig. 3b shows an individual result for the third trial of the 25 BC GDL at a stoichiometry of 2, with the error bars representing the standard deviation of the individual data set.

The ascending case has a small percentage error (ratio of standard deviation to overall pressure drop). The high percentage error

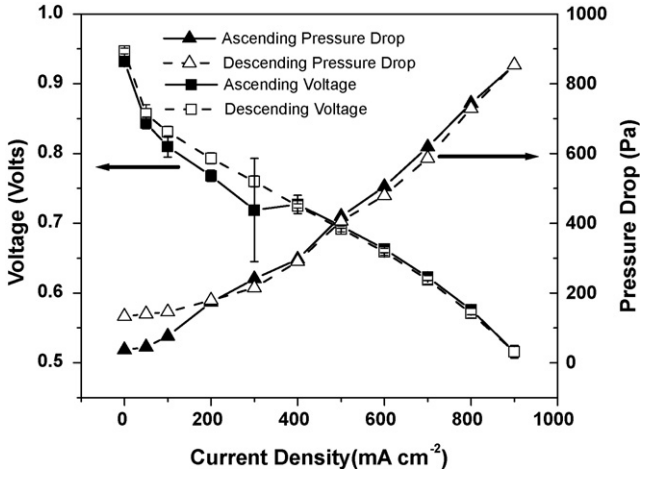

Fig. 2. Ascending and descending pressure drops from an operational fuel cell.

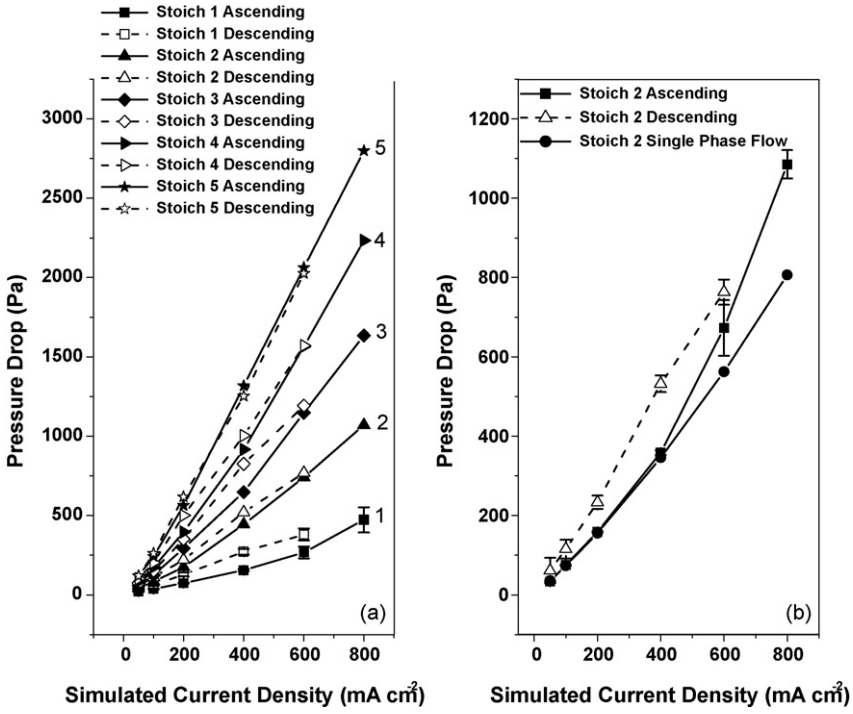

Fig. 3. (a) Effect of gas stoichiometry on two-phase pressure drop hysteresis for the 25 BC GDL [P_{gas} = 0 kPa$_g$, T_{gas} = ambient, dry air]. (b) Individual trial result at a stoichiometry of 2.

at low simulated current densities during the descending approach is a result of the large oscillations in signal due to the flow type. More discussion on the signal fluctuations is in Section 3.5.

The ascending pressure drop and descending pressure drop are not identical for stoichiometries in the range of 1–4. At a stoichiometry of 5, however, the pressure drops from flow ascending and descending match each other. This pressure drop hysteresis effect can be explained by how water enters and leaves the cathode flow field channels. At low simulated current densities, no water is being introduced and the fluid flow in the channels is essentially single-phase flow. Fig. 3b shows the results for single phase flow (air only) with the 25 BC GDL at a stoichiometry of 2, which illustrates how the ascending pressure drop and single phase pressure drop are the same when the simulated current density is less than or equal to 400 mA cm^{-2}. Water breakthrough is evident at a higher simulated current density greater than or equal to 600 mA cm^{-2}. In this setup, it is not until these rates that a critical breakthrough pressure is reached, as discussed by Bazylak et al. [9]. As the air flow is lowered in the descending approach, the injected water is unable to be removed from the channels quickly, and the residual water causes a higher pressure drop. This argument is true for lower stoichiometries that are less than or equal to four. At stoichiometries of 5 and higher, the air flow is sufficient to remove all injected water and, as a result, residual water is not accumulated. Due to the equilibrium addition and quick removal of water, the ascending and descending pressure drops do not display a hysteresis in this higher stoichiometric range.

The extent of pressure drop hysteresis can be quantified by the percentage change between the ascending and descending pressure drops, as shown in Fig. 4. The percentage change is defined as

$$\%\ \text{Change} = \left[\frac{\Delta P_{\text{Descending}} - \Delta P_{\text{Ascending}}}{\Delta P_{\text{Ascending}}}\right] \times 100 \qquad (3)$$

A higher percentage change from ascending to descending pressure drops indicates a more pronounced difference between the descending and ascending pressure drop.

Three different regions are drawn in this figure for illustrative purposes. At a stoichiometry of 1, the hysteresis effect is large for all simulated current densities because the low air flows are unable to remove the residual water in the descending case (Region 1). Operation for stoichiometries in the range of 2–4 falls into Region 2, where the hysteresis effect is not noted at high current densities ($\geq$600 mA cm^{-2}). However, at lower simulated current densities the air is unable to remove residual water in the descending case and two-phase flow hysteresis appears. For a higher stoichiometry of 5 (Region 3), the hysteresis effect is eliminated because the air flow is sufficiently high to prevent the accumulation of residual water. In this region, the percentage change between ascending and descending pressure drop is consistently below 10%.

3.3. Effect of GDL type: hydrophobicity and microporous layer

The GDL serves as the main barrier to water entering the flow field channels of operating fuel cells, and the specific GDL can affect

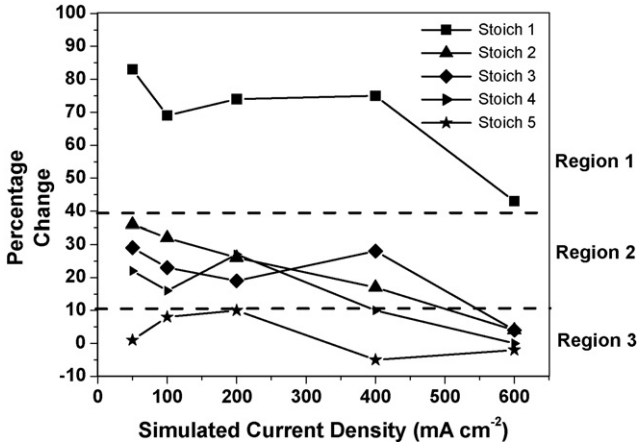

Fig. 4. Percentage change in ascending and descending pressure drops.

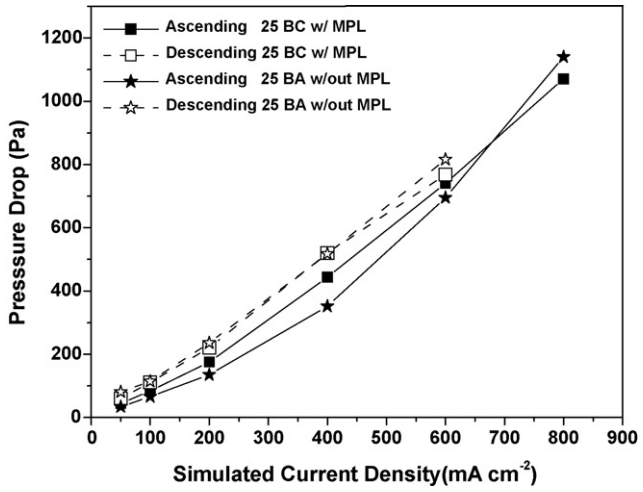

Fig. 5. Effect of MPL: SGL 25 BC and 25 BA at a stoichiometry of 2 [P_{gas} = 0 kPa$_g$, T_{gas} = ambient, dry air].

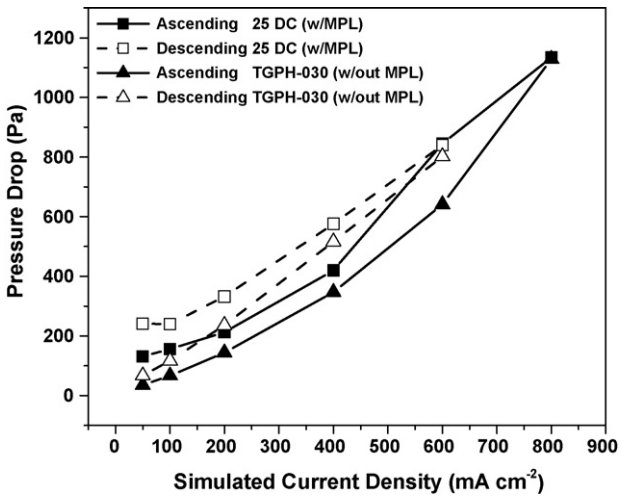

Fig. 6. Effect of MPL: 25 DC vs. TGPH-030 20% PTFE at a stoichiometry of 2 [P_{gas} = 0 kPa$_g$, T_{gas} = ambient, dry air].

the water flux through the GDL into the flow field channels [21]. Five different GDLs were tested and compared at a stoichiometry of 2 (the baseline cathode stoichiometry for the operational fuel cell). These GDLs were chosen to investigate the effect of a microporous layer (MPL) and PTFE content on flow and hysteresis. Lee et al. [18] have shown these parameters to have an impact on observed flow regime in fuel cell flow channels. The GDLs used in this research and their relevant specifications are shown in Table 1.

3.3.1. *Effect of the MPL*

Fig. 5 shows the effect of the MPL by comparing SGL 25 BC (with MPL) and 25 BA (without MPL), which have the same PTFE treatment but a different thickness due to the inclusion of an MPL.

These results show that both GDLs share the same descending pressure drop but different ascending pressure drops. At the same air flow, the similar capability of expelling the residual water suggests that the droplet detachment/removal dynamics are similar for the two types of GDLs, which have the same PTFE content. The ascending pressure drop for the 25 BA GDL (no MPL) is lower, leading to a larger hysteresis zone. This result is because the available cross-sectional area of the thicker GDL (25 BC) was reduced upon compression, an effect noted previously in numerical simulations [22]. This effect would lead to a higher ascending pressure drop at lower simulated current densities, where the effect of water breakthrough is not large. This result was confirmed in a single-phase compression study with the 25 BC and 25 BA GDLs (dry gas, T = ambient, $\lambda = 2$, P_{gas} = 0 kPa$_g$). From 0 to 100 psi$_g$ compression pressure, the single phase pressure drop increased by an average of 24% for the 25 BC GDL and only 5% for the 25 BA GDL over the ranged of simulated current densities tested.

The effect of the MPL on two-phase flow hysteresis was also studied by comparing the 25 DC (20% PTFE, MPL) and TGPH-030 with 20% PTFE GDL (no MPL). These results at a stoichiometry of 2 are shown in Fig. 6.

Both GDLs exhibit pressure drop hysteresis. The onset of two-phase flow hysteresis happens at a higher current density and the extent of the hysteresis is also greater for the GDL without MPL. Table 3 shows the percentage change between the ascending and descending case for the four GDLs. The data shows that the 25 DC GDL and 25 BC GDL (both with MPL) allow for water breakthrough at a lower simulated current density, which correlates to the enhanced liquid water removal abilities of the MPL discussed by Pasaogullari et al. [23]. Water breakthrough at lower simulated current densities reduces the difference between the ascending and descending pressure drop. The later injection during the ascending approach leads to a lower ascending pressure drop and therefore more hysteresis once the water breaks through for the GDLs with no MPL.

3.3.2. *Effect of hydrophobicity*

Fig. 7b–d show the effect of PTFE treatment by comparing TGPH-030 with 0% PTFE, TGPH-030 with 20% PTFE, and 25 BA with 5% PTFE, respectively. The single phase pressure drop result for each GDL is also included to show the influence of two-phase flow on the pressure drop.

Water breaks through the GDL with no PTFE at a lower flow rate than the PTFE coated GDLs, leading to a higher ascending pressure drop. Due to the higher pressure drop in the ascending case, the hysteresis effect is only noted for the plain GDL at simulated current densities of 200 mA cm^{-2} and lower. The prolonged breakthrough with the TGPH-030 20% PTFE coated GDL led to a lower ascending pressure drop and therefore a wider hysteresis zone. At current densities below 200 mA cm^{-2}, the plain GDL also exhibits a larger pressure drop in the descending approach compared to the TGPH-030 20% PTFE coated GDL. This is a result of the reduced PTFE content, which hinders the droplet's detachment from the GDL surface due to higher hydrophilicity (wetting of the surface) [24]. The 25 BA GDL shows very similar results to the TGPH-030 20%

Table 3
Percent change in pressure drop between the ascending and descending approach.

Simulated current density (mA cm^{-2})	% change for the 25 BC GDL	% change for the 25 DC GDL	% change for the 25 BA GDL	% change for the TGPH-030 20% PTFE GDL
50	36	85	140	90
100	32	54	72	73
200	26	57	75	64
400	17	37	47	49
600	4	−1	17	25

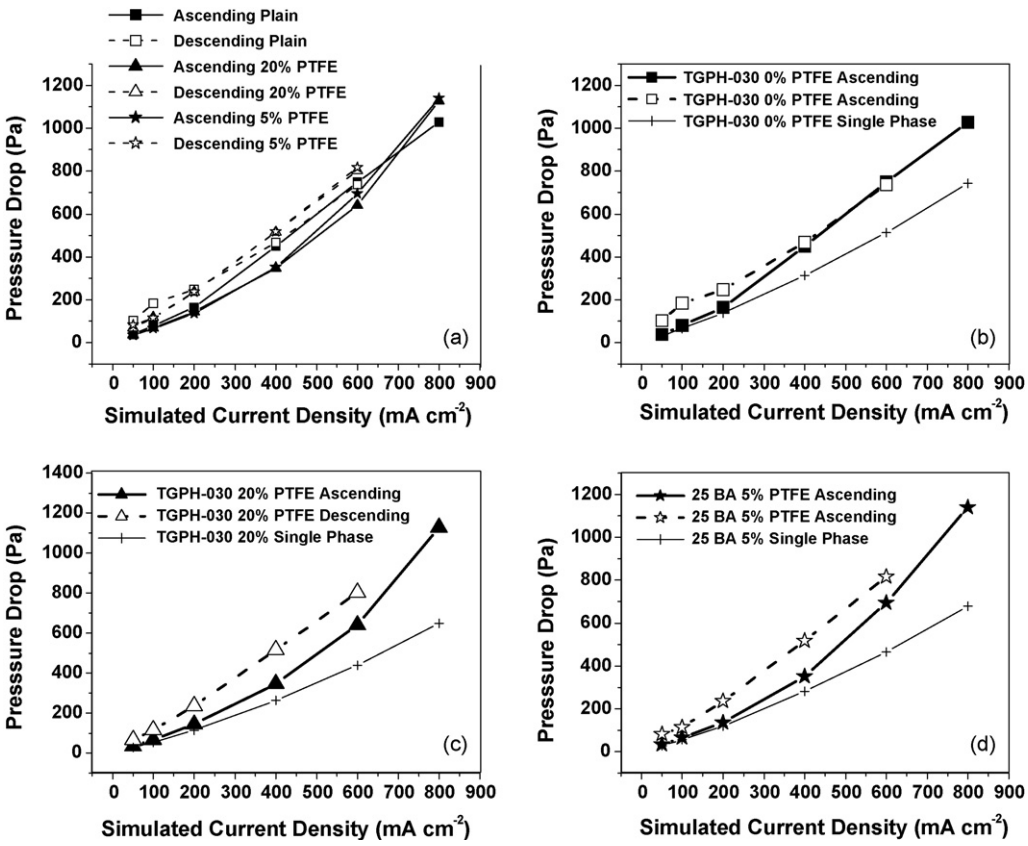

Fig. 7. Effect of PTFE treatment: (a) three GDLs, (b) TGPH-030 with 0% PTFE, (c) TGPH-030 with 20% PTFE and (d) 25 BA with 5% PTFE [P_{gas} = 0 kPa$_g$, T_{gas} = ambient, dry air].

PTFE coated GDL. The percentage difference between these GDLs, defined as

$$\%\ \text{Change}_{\text{GDLs}} = \left[\frac{\Delta P_{25\text{BA}} - \Delta P_{\text{TGPH-030,20\%}}}{\Delta P_{25\text{BA}}}\right] \times 100 \quad (4)$$

is on average less than 4%. This result indicates that additional PTFE (20% vs. 5%) does not influence the extent of the hysteresis.

3.4. Effect of simulated current density range

The range over which the simulated current density was varied is explored in this section by studying the effect of an ascending approach up to 400 mA cm^{-2} and up to 1600 mA cm^{-2}. The baseline GDL (SGL 25 BC) and baseline operating conditions (dry gas, ambient temperature, $\lambda = 2$) were used in this study. The results for the final ascending current densities to 1600, 800, and 400 mA cm^{-2} are shown in Fig. 8a–c, respectively.

If a minimum water injection rate is not reached, as in the case of 400 mA cm^{-2}, there is no breakthrough so no hysteresis is observed. For a final current density of 800 mA cm^{-2}, the breakthrough of water causes accumulation that cannot be removed effectively by the descending airflow, leading to hysteresis. The case of 1600 mA cm^{-2} follows the same hysteresis behavior in the same zone as the 800 mA cm^{-2} case. However, above a current density of 800 mA cm^{-2} the air flow is able to remove the injected water at a sufficient rate. An equilibrium between air flow, water injection rate, and accumulation is established so that there is no hysteresis effect in the high flow rate range. Below 600 mA cm^{-2}, an equilibrium no longer exists (as in Fig. 8a). Accumulated water in the channels at lower air flows (below 600 mA cm^{-2}) causes a higher pressure drop in the descending case, establishing two-phase hysteresis.

3.5. Effect of descending step size

In the previous experiments, the simulated current density was incrementally increased to 800 mA cm^{-2} and then descended along the same path (600, 400, 200, 100, 50 mA cm^{-2}). Four trials were run to analyze the effect of the initial descending step size. Each experiment began at 800 mA cm^{-2} (no ascending approach), and the descending approach step size was changed with each simulated current density held for approximately 8 min. The experimental approaches are given in Table 4.

Each cluster of results in Fig. 9 shows the total difference in pressure drop between the pressure drop at 800 mA cm^{-2} and the pressure drop at each current density, i.e. $\Delta P_{800\,\text{mA cm}^{-2}} - \Delta P_{50\,\text{mA cm}^{-2}}$. For example, 800 → 50 mA cm^{-2} contains five boxes since each trial ended at 50 and 800 → 600 mA cm^{-2} only has one box since only one trial includes the 600 mA cm^{-2} operating point.

The results show that the decrease in pressure drop from the pressure drop at 800 mA cm^{-2} to each lower current density is similar within experimental error regardless of the size of the jump. For example, the pressure drop at 50 mA cm^{-2} is the same whether the path goes from 800 → 400 → 200 → 100 → 50 mA cm^{-2} or from 800 → 50 mA cm^{-2}. This result implies that the balance of water introduced and subsequently accumulated at each operating con-

Table 4
Descending approach experiments on the effect of step size.

Trial number	Descending approach (mA cm^{-2})
0 (previous baseline)	800 → 600 → 400 → 200 → 100 → 50
1	800 → 400 → 200 → 100 → 50
2	800 → 200 → 100 → 50
3	800 → 100 → 50
4	800 → 50

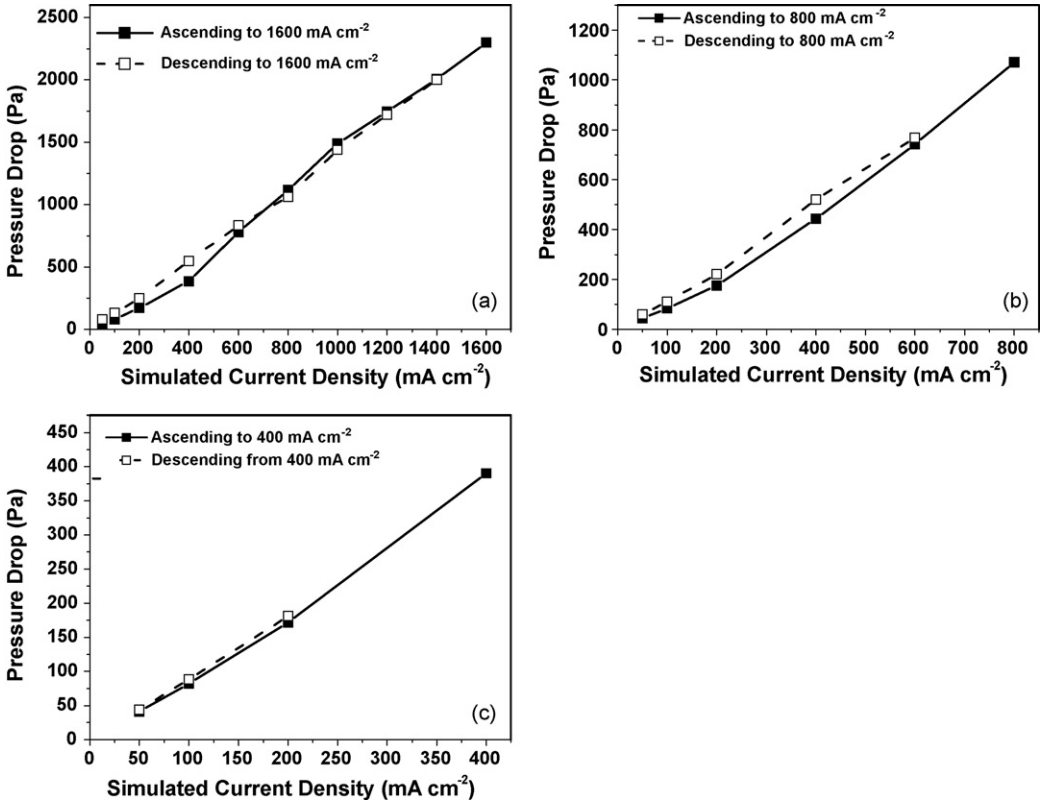

Fig. 8. Final current density: (a) 1600 mA cm^{-2}, (b) 800 mA cm^{-2} and (c) 400 mA cm^{-2} [P_{gas} = 0 kPa$_g$, T_{gas} = ambient, dry air].

dition quickly reaches equilibrium. However, the dynamic behavior of the pressure drop signals is different depending on the size of the descending step change, as reflected in the pressure drop signals shown in Fig. 10 for the two cases.

The average pressure drops within the standard deviation of the data set are similar despite clearly different dynamic behavior. However, when a multi-step approach is used (800 to 400, 200, 100, 50 mA cm^{-2}), the resulting pressure drop at 50 mA cm^{-2} fluctuates much more than the single-step approach to 50 mA cm^{-2} from 800 mA cm^{-2}. From visual inspection using the optical window in the fuel cell, no noticeable difference was observed in the flow pattern and no large slugs were noticeable. For practical fuel cell operation, it would be useful to have a stable pressure drop signal, and thus the step size during operational changes should be considered.

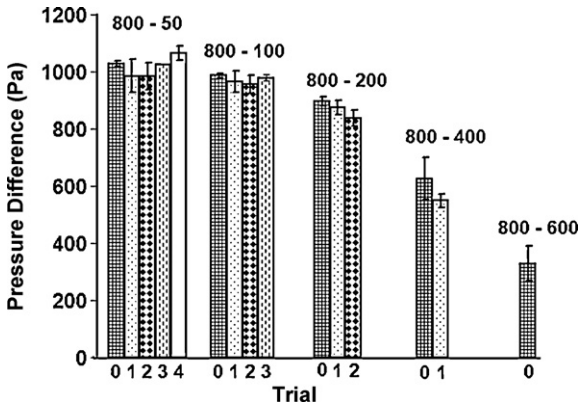

Fig. 9. Difference in pressure drop from the 800 mA cm^{-2} pressure drop.

3.6. *Effect of an initially flooded state*

All previous experiments began with dry cathode flow field channels. However, it is also important to explore the pressure drop hysteresis when the channels are already flooded since the current density of an operational fuel cell could be changed in either an ascending or descending manner once water is already in the channels. Initial flooding in the channels was accomplished by injecting the cathode flow channel full of water. The initial condition in all flooding cases quickly became a combination of droplets on the GDL surface, liquid slugs (water droplet touching all four walls), and annular droplets (water film on the gold-coated channel walls).

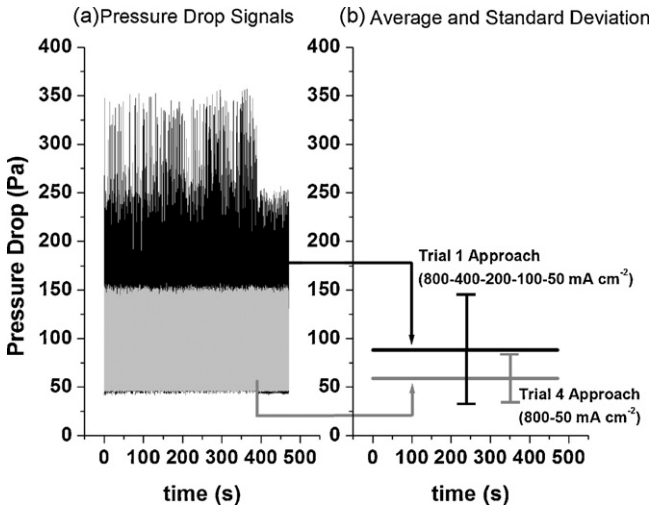

Fig. 10. Pressure fluctuation signals for two approaches to 50 mA cm^{-2}: (a) pressure drop signals, and (b) average and standard deviation.

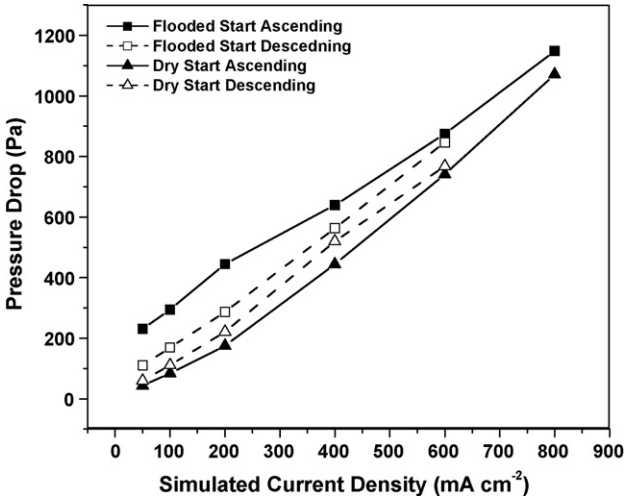

Fig. 11. Effect of initial condition: dry vs. flooded for the SGL 25 BC GDL [P_{gas} = 0 kPa$_g$, T_{gas} = ambient, dry air].

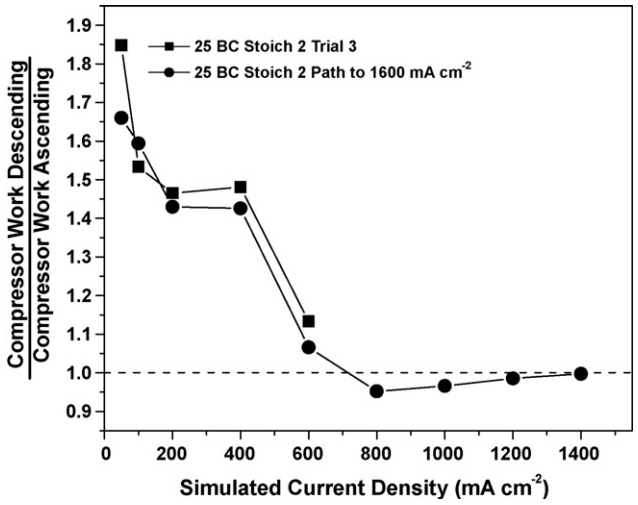

Fig. 12. Ratio of compressor work for the descending to ascending approach.

The initially flooded case exhibited pressure drop hysteresis, but the ascending pressure drop was higher than the descending case. This result is the opposite of the dry start case. A typical case is shown in Fig. 11 for the SGL 25 BC GDL at an air stoichiometry of 2.

In the dry start case, the pressure drop for the ascending case is lower than the descending case because the accumulated water from the ascending approach could not be removed by the lower air flow rates in the descending case. Since the amount of water initially present in the flooded channels is greater than the amount accumulating from water breakthrough after a dry start, the ascending pressure drop for a flooded start was higher than the initially dry ascending or descending pressure drop. Once a sufficient air flow is reached in the initially flooded ascending case (e.g. $\lambda = 2$, $i = 800\,mA\,cm^{-2}$), most of the initial water is expelled from the channels. The remaining water is from the breakthrough process and therefore the descending pressure drops are similar for the dry and flooded start. Similar results were observed with the SGL 25 BC (5% PTFE) and TGPH-030 (20% PTFE) GDLs. In both cases, the ascending pressure drop was higher than the descending pressure drop when the channels were initially flooded. However, a difference was observed with the plain TGPH-030 (0% PTFE) GDL. The less hydrophobic nature of this GDL did not facilitate water removal like the others and no hysteresis effect was noted between the ascending and descending cases of the initially flooded experiments.

All of these specific results also depend on the surface wettability of the landings and channel walls. Bazylak et al. [25] studied surface wettability and showed a hydrophilic solid surface, like the gold-coated flow field used in the current study, favors droplet spreading and liquid water entrapment between the GDL and landing width. These observations help explain why water spreads in the initial startup of the flooded experiments. In addition, land touching droplets tend to grow faster in an operating fuel cell as shown by Ous et al. [26], which complicates the water removal mechanism and can influence the pressure drop.

4. Implications in the operating fuel cell

These results have practical implications in operating fuel cells. The additional pressure drop due to hysteresis means that more power is needed for the compressor to supply air, resulting in a parasitic power loss. These parasitic losses must be avoided for the fuel cells to obtain high overall efficiency, confirming the importance of proper water management in the flow field channels of PEM fuel cells. The ideal power [27] for an adiabatic compressor to increase the air pressure from P_1 to P_2 is

$$W_{comp,ideal} = \dot{m}_{air,in} \cdot c_p \cdot T_1 \left[\left(\frac{P_2}{P_1} \right)^{(k-1)/k} - 1 \right] \quad (5)$$

Thus, any situation resulting in a higher pressure drop will lead to a higher parasitic power loss. A ratio of the work needed for an ideal compressor between the ascending and descending case for two experiments are shown in Fig. 12. The first experiment refers to the third trial of the 25 BC GDL at a stoichiometry of two (Fig. 3b) and the second case refers to the maximum current density reaching 1600 mA cm^{-2} with the 25 BC GDL at a stoichiometry of 2 (Fig. 8a).

A ratio greater than one means more work is needed to supply the appropriate air flow during the descending path, which means a higher parasitic power loss. Above 800 mA cm^{-2}, there is no increase in compressor work but below 600 mA cm^{-2}, the ratio is greater than one due to the hysteresis effect. Additional mechanical and electrical inefficiencies make the actual parasitic power loss even higher. The hysteresis effect was eliminated in the non-operating experiments at a high stoichiometry of 5, but this would result in 5 times the power needed for the compressor due to the increased mass flow of air.

5. Conclusions and future work

Two-phase flow pressure drop hysteresis was studied in a fuel cell under non-operating conditions at ambient temperature and without humidification to establish a hydrodynamic baseline for the fuel cell. Hysteresis is noted when the air flow rate and water injection rate (determined from Faraday's law) are increased and then decreased along the same path, but exhibit different pressure drops. These results are relevant to fuel cell applications that experience a load cycle, such as automotive applications, where an additional pressure drop would increase the parasitic power loss of the system. Initially, little water is able to enter the channel because the pressure barrier through the GDL is too high. At sufficiently high current densities, enough water is forced into the cathode flow field channels to cause water accumulation. As the air flow rate decreases along the same path, the water is not sufficiently expelled and remains in the channels, causing a pressure drop hysteresis between the ascending and descending cases. The following conclusions were drawn from the non-operating experiments:

1. Two-phase flow hysteresis is eliminated at stoichiometries of 5 and higher. Sufficient air flow is able to remove the water entering the channels in the ascending and descending case at

this stoichiometry, leaving no residual water to induce a two-phase pressure drop hysteresis. However, a high air flow rate also requires additional work from the air compressor.

2. The inclusion of an MPL and PTFE coating changes the ascending pressure drop. The MPL leads to a thicker GDL, which can reduce the cross-sectional area upon compression and therefore increase the pressure drop. Water is able to break through the GDLs with the MPL at lower ascending current densities, reducing the size of the hysteresis zone. PTFE facilitates water removal and reduces the extent of the hysteresis, which can be seen at lower current densities (<200 mA cm^{-2}) where the TGPH-030 0% PTFE GDL has a higher descending pressure drop than the 25 BA (5% PTFE) and TGPH-030 20% PTFE coated GDLs.
3. Two-phase flow hysteresis is noted only once a critical water injection rate (simulated current density) is reached to allow sufficient water to enter the channels. Also, high current densities have a high enough air flow rate to remove the same amount of water in the ascending and descending case. Thus, a hysteresis zone is only noted when enough water has entered the channels and the subsequent air flow is too low for water to be removed. In the current study, conditions equivalent to a critical current density of 800 mA cm^{-2} were identified as necessary for a hysteresis zone.
4. The step size in the descending approach does not affect the magnitude of the two-phase flow pressure drop hysteresis. However, the pressure drop signal with a large decreasing step size shows lower fluctuations than the signal with more small steps.
5. The hysteresis effect is inverted when the channel is initially flooded for the 25 BA, 25 BC, and TGPH-030 with 20% PTFE GDLs. When water is initially in the channels, the ascending pressure drop is higher than the descending case since the air flow at low current densities is insufficient to remove the original water. In the initially dry or flooded cases, the same descending pressure drop is noted. An exception to this is the non-treated GDL (TGPH-030 0% PTFE), where no hysteresis is noted for an initially flooded case. The water initially present in this case does not detach from the GDL surface, which creates the same flooding condition, and therefore the same pressure drop, in both the ascending and descending approach.

Work is currently being continued in our lab on studying two-phase flow hysteresis with humidified and heated gases now that a hydrodynamic baseline has been established. This work will serve as a further step toward the goal of studying two-phase flow hysteresis in an operating (electrochemically active) fuel cell, where the hydrodynamic results can be analyzed in correlation to the fuel cell performance.

Acknowledgements

The authors are grateful for a strategic grant from the Natural Sciences and Engineering Research Council of Canada (NSERC) to support this work. Ryan Anderson is also grateful for a university graduate scholarship (UGF) from the University of British Columbia.

References

[1] H. Li, Y. Tang, Z. Wang, Z. Shi, S. Wu, D. Song, J. Zhang, K. Fatih, J. Zhang, H. Wang, Z. Liu, R. Abouatallah, A. Mazza, J. Power Sources 178 (2008) 103–117.
[2] T.A. Trabold, Heat Transfer Eng. 26 (2005) 3–12.
[3] S.G. Kandlikar, Heat Transfer Eng. 29 (7) (2008) 575–587.
[4] A. Marchitto, F. Devia, M. Fossa, G. Guglielmini, C. Schenone, Int. J. Multiphase Flow 34 (2008) 128–144.
[5] K. Pehlivan, I. Hassan, M. Vaillancourt, Appl. Therm. Eng. 26 (2006) 1506–1514.
[6] J.S. Allen, ECS Trans. 3 (1) (2006) 1197–1206.
[7] Y. Taitel, L. Pustylnik, M. Tshuva, D. Barnea, Int. J. Multiphase Flow 29 (2003) 1193–1202.
[8] J. Borrelli, T. Trabold, S. Kandlikar, J. Owejan, in: Proceedings of the Third Annual Conference on Microchannels and Minichannels, June 13–15, 2005.
[9] A. Bazylak, D. Sinton, N. Djilali, J. Power Sources 176 (1) (2008) 240–246.
[10] Z. Lu, A.D. White, J. Pelaez, M. Hardbarger, W. Domigan, J. Sergi, S.G. Kandlikar, in: Proceedings of the Sixth International ASME Conference on Nanochannels, Microchannels, and Minichannels, June 23–25, 2008.
[11] I.S. Hussaini, C.-Y. Wang, J. Power Sources 187 (2) (2009) 444–451.
[12] E. Kimball, T. Whitaker, Y. Kevrekidis, J. Benziger, AIChE J. 54 (2008) 1313–1332.
[13] X. Liu, H. Guo, F. Ye, C.F. Ma, Int. J. Hydrogen Energy 33 (2008) 1040–1051.
[14] Z. Lu, S.G. Kandlikar, C. Rath, M. Grimm, W. Domigan, A.D. White, M. Hardbarger, J.P. Owejan, T.A. Trabold, Int. J. Hydrogen Energy 34 (2009) 3445–3456.
[15] H.P. Ma, H.M. Zhang, J. Hu, Y.H. Cai, B.L. Yi, J. Power Sources 162 (2006) 469–473.
[16] L.F. Zhang, H.T. Bi, D.P. Wilkinson, J. Stumper, H.J. Wang, J. Power Sources 183 (2) (2008) 643–650.
[17] L.F. Zhang, W. Du, H.T. Bi, D.P. Wilkinson, J. Stumper, H.J. Wang, J. Power Sources 189 (2009) 1023–1031.
[18] E.S. Lee, C. Hidrovo, K. Goodson, J. Eaton, in: 6th International Conference on Multiphase Flow, Leipzig, Germany, July, 2007, Paper No. S7_Thu_A_46.
[19] USFCC Joint Hydrogen Quality Task Force, USFCC 04-068 Rev. A_2006_.
[20] F.-B. Weng, A. Su, C.-Y. Hsu, Int. J. Hydrogen Energy 32 (2007) 666–676.
[21] W. Dai, H. Wang, X.Z. Yuan, J.J. Martin, Z. Luo, M. Pan, J. Power Sources 185 (2008) 1267–1271.
[22] S. Basu, J. Li, C.-Y. Wang, J. Power Sources 187 (2) (2009) 431–443.
[23] U. Pasaopullari, C.-Y. Wang, Electrochim. Acta 49 (2004) 4359–4369.
[24] E.C. Kumbur, K.V. Sharp, M.M. Mench, J. Power Sources 161 (2006) 333–345.
[25] A. Bazylak, J. Heinrich, N. Djilali, D. Sinton, J. Power Sources 185 (2) (2008) 1147–1153.
[26] T. Ous, C. Arcoumanis, J. Power Sources 173 (2007) 137–148.
[27] F. Barbir, PEM Fuel Cells: Theory and Practice, Elsevier Academic Press, New York, 2005.